

Two-Loop Threshold Singularities, Unstable Particles and Complex Masses ^{‡‡}

STEFANO ACTIS ^{*}

*Institut für Theoretische Physik E, RWTH Aachen University,
52056 Aachen, Germany*

GIAMPIERO PASSARINO [†]

*Dipartimento di Fisica Teorica, Università di Torino, Italy
INFN, Sezione di Torino, Italy*

CHRISTIAN STURM [‡]

*Physics Department, Brookhaven National Laboratory,
Upton, NY 11973, USA*

SANDRO UCCIRATI [§]

*Institut für Theoretische Teilchenphysik, Universität Karlsruhe,
76128 Karlsruhe, Germany*

The effect of threshold singularities induced by unstable particles on two-loop observables is investigated and it is shown how to cure them working in the complex-mass scheme. The impact on radiative corrections around thresholds is thoroughly analyzed and shown to be relevant for two selected LHC and ILC applications: Higgs production via gluon fusion and decay into two photons at two loops in the Standard Model. Concerning Higgs production, it is essential to understand possible sources of large corrections in addition to the well-known QCD effects. It is shown that NLO electroweak corrections can incongruently reach a 10% level around the WW vector-boson threshold without a complete implementation of the complex-mass scheme in the two-loop calculation.

Keywords: Feynman diagrams, Multi-loop calculations, Higgs physics

PACS classification: 11.15.Bt, 12.38.Bx, 13.85.Lg, 14.80.Bn, 14.80.Cp

^{‡‡}Work supported by MIUR under contract 2001023713_006, by the European Community's Marie Curie Research Training Network *Tools and Precision Calculations for Physics Discoveries at Colliders* under contract MRTN-CT-2006-035505, by the U.S. Department of Energy under contract No. DE-AC02-98CH10886 and by the Deutsche Forschungsgemeinschaft through Sonderforschungsbereich/Transregio 9 *Computergestützte Theoretische Teilchenphysik*. The authors thank the Galileo Galilei institute for Theoretical Physics for hospitality and the INFN for partial support during the completion of this work.

^{*}actis@physik.rwth-aachen.de

[†]giampiero@to.infn.it

[‡]sturm@bnl.gov

[§]uccirati@particle.uni-karlsruhe.de

1 Introduction

The computation of higher order corrections to multi-scale processes is plagued by the presence of unstable particles in loop integrals. Formally, a clean description would require a Dyson resummation of self-energy insertions in order to preserve unitarity [1]; in the context of the Standard Model and its extensions, however, the consequent mixing of perturbative orders clearly compromises gauge invariance. In addition to the unitarity issue, a practical problem is represented by the appearance of unphysical threshold singularities at the amplitude level for physical observables.

In this letter we focus on two-loop electroweak corrections to Standard Model Higgs production through gluon fusion, $gg \rightarrow H$, and decay into two photons, $H \rightarrow \gamma\gamma$ (details of the calculation will be given in a forthcoming paper [2]). We discuss the singular behavior of the amplitudes around the normal thresholds induced by internal unstable particles, directly related to two-particle unitarity cuts. Concerning the $H \rightarrow \gamma\gamma$ case, note that threshold effects have been analyzed in Ref. [3], with special emphasis on the presence of bound states, which are not the subject of our study.

The singular behavior can be cured trading the real masses for unstable particles, used as experimental input data, with the associated complex poles. As shown by the authors of Ref. [4], the replacement has to be performed also at the level of the couplings, leading to the so-called complex-mass scheme. Consequently, the one- and two-loop integrals needed for the computation have to be evaluated with complex internal arguments.

A minimal implementation of the complex-mass scheme for two-loop electroweak corrections to the $H \rightarrow \gamma\gamma$ process has been realized in Ref. [5]. The two-loop amplitude is splitted in gauge-invariant divergent and non-divergent terms, and complex masses are introduced in the divergent part. This solution is formally satisfactory, since the amplitude is finite also at thresholds. Furthermore, as a consequence of the cancellation mechanism taking place among divergent contributions, this scheme does not require any analytic continuation of two-point functions connected to mass renormalization to the second Riemann sheet.

As a drawback, artificially large numerical effects arise around normal thresholds. The issue is relevant when we consider Higgs production through gluon fusion at the LHC, where a measurement of the Higgs mass can be performed at the per-mille level [6]. The statement that next-to-leading order electroweak corrections are known [7] does not appear to be fully adequate, given the possible occurrence of large threshold effects of about 10% with respect to the leading order result.

In this letter we show that threshold effects for $gg \rightarrow H$ and $H \rightarrow \gamma\gamma$ are well under control in our improved calculational scheme [2], where a complete implementation of the complex-mass scheme at two loops is performed along the lines of Ref. [8]. For the analysis in hadron-hadron collisions we refer to Ref. [9].

2 Radiative corrections with unstable particles

In this section we briefly summarize aspects of selected solutions for dealing with unstable particles in tree and one-loop calculations; next, we analyze the salient features of a two-loop computation. In Section 3 we will study where the numerical impact of complex masses is most relevant at the two-loop level by looking into the presence of unphysical infinities and cusps in two-loop amplitudes.

At tree level, if the external legs of a given amplitude are divided into two disjoint subsets and if the total quantum numbers of each subset allow for the exchange of a known particle of mass M , then the amplitude has a pole satisfying $p^2 = M^2$, where p is the four-momentum of the exchanged

particle. In leading order (LO) calculations, the masses of these particles, like W and Z bosons, are replaced by the location of the poles in the complex p^2 plane. However, the principle of gauge invariance must not be violated: in particular, Ward-Slavnov-Taylor (hereafter WST) identities [10] have to be preserved, otherwise theoretical uncertainties may get out of control. The incorporation of finite-width effects in the theoretical predictions for Lep2 processes was a typical example and, at the time, it was argued that the preferable scheme consists in resummation of fermion one-loop corrections to vector-boson propagators and inclusion of all remaining fermion one-loop corrections, in particular those to the Yang-Mills vertices [11].

A possible solution at the next-to-leading order (NLO) level consists in replacing everywhere the squared real masses (m^2) with the complex poles (s_P), couplings included; this is known in the literature as complex-mass scheme [4]. Since WST identities are algebraic relations satisfied separately by real and imaginary parts, one starts from WST identities with real masses, satisfied at any given order, and replaces everywhere $m^2 \rightarrow s_P$ without violating the invariance.

In turns, this scheme violates unitarity: one cannot identify the two sides of any cut diagram with T and T^\dagger respectively (the transition matrix T is defined in terms of the S matrix as $S = 1 + iT$). To summarize, the analytical structure of the S matrix is correctly reproduced when we use propagator factors $s - s_P$, where s is a generic invariant, but unitarity of S requires more, a dressed propagator [8, 12]. However, we expect that unitarity-violating terms are of higher order; in principle, the violating terms should not be enhanced because WST identities are preserved.

Another drawback of the scheme is that all propagators for unstable particles will have the same functional form both in the time-like and space-like regions, while, for a dressed propagator, the presence of a pole on the second Riemann sheet does not change the real character of the function if we are in a t channel.

Typical examples of one-loop calculations that require the introduction of complex poles are those for processes, like $e^+e^- \rightarrow 4f$, where part of the amplitude (the so-called signal) factorizes into production \otimes decay of one or more particles; or processes involving off-shell W -pair production, leading to the so-called Coulomb singularity. Another approach in this context is represented by the use of effective field theory methods (see recent applications in Ref. [13]).

In some sense the complex-mass scheme becomes more appealing when we go beyond one loop, as described in detail in Ref. [8], where a recipe was designed to derive loop amplitudes out of a skeleton expansion. Let m^2 be the squared bare mass, s_P the corresponding complex pole and Σ the corresponding self-energy: to the requested order we replace everywhere m^2 with $s_P + \Sigma(s_P)$, which is real by construction. If only one loop is needed, then $m^2 \rightarrow s_P$ everywhere (therefore justifying the name *complex mass*).

Note that the on-shell mass is related to the zero of the real part of the inverse propagator; beyond one loop this would show a clash with gauge invariance, since only the complex poles do not depend on gauge parameters to all orders. As a consequence, renormalization equations change their structure.

Furthermore, there is also a change of perspective with respect to one-loop calculations. There one considered the on-shell masses as input parameters independent of complex poles and derived the latter in terms of the former [11]. Here the situation changes: renormalization equations are written for real renormalized parameters and solved in terms of (among other things) experimental complex poles; the latter have to be reconstructed from on-shell pseudo-observables.

Having described the general setup for a gauge-invariant formulation of unstable particles at the multi-loop level, we want to understand where, in a two-loop calculation, the numerical impact of complex masses is most relevant.

3 Two-loop amplitudes and normal thresholds

In this section we explore the singular behavior of massive two-loop amplitudes around normal thresholds, investigating the origin of square-root and logarithmic singularities. It is worth noting that pseudo-thresholds are always outside the physical region.

Normal thresholds are directly related to unitarity cuts as illustrated in Fig. 1, and correspond to the leading Landau singularities [14] of self-energy diagrams. When diagrams with more than two external legs are present, normal thresholds show up as sub-leading singularities; this can be easily understood observing that all diagrams in Fig. 1 are reduced to self-energy configurations after shrinking a line which does not intersect any cut to a point.

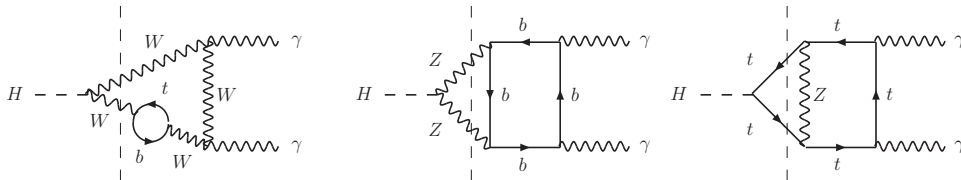


Figure 1: Sample cut diagrams for $H \rightarrow \gamma\gamma$ showing normal thresholds for $M_H = 2M_W, 2M_Z, 2M_t$.

An interesting question is the role played by the leading singularity (the so-called anomalous threshold) [15]: already at one loop, there are cases where a non-integrable singularity associated with the leading Landau singularity requires the introduction of complex masses [16]. Concerning the processes $H \rightarrow \gamma\gamma$ and $gg \rightarrow H$, we have verified that the leading Landau singularities of all two-loop vertex diagrams lie outside the physical region, and we will drop this issue in the following.

For our discussion, it is useful to decompose the $H \rightarrow \gamma\gamma$ amplitude as

$$\mathcal{A} = \left(\sqrt{2} G_F M_W^2\right)^{1/2} \frac{\alpha}{2\pi} \left(\mathcal{A}^{\text{LO}} + \frac{G_F M_W^2}{2\sqrt{2} \pi^2} \mathcal{A}^{\text{NLO}} \right), \quad (1)$$

where G_F is the Fermi-coupling constant, M_W is the mass of the W boson and α is the fine-structure constant; \mathcal{A}^{LO} and \mathcal{A}^{NLO} denote the leading order and next-to-leading order amplitudes. Furthermore, \mathcal{A}^{NLO} can be written as

$$\mathcal{A}^{\text{NLO}} = \mathcal{A}^{2\text{L}} + \mathcal{A}^{\text{REN}} + \mathcal{A}^{\text{WFR}}, \quad (2)$$

where $\mathcal{A}^{2\text{L}}$ is given by the sum of all pure two-loop diagrams, \mathcal{A}^{WFR} follows from the inclusion of the one-loop Higgs wave-function renormalization (WFR) factor and \mathcal{A}^{REN} stems from one-loop renormalization of the masses and the Fermi coupling. Note that the U(1) Ward identity forces the electromagnetic coupling to go unrenormalized once the external on-shell photons are provided with their WFR factors. For electroweak corrections, the amplitude for $gg \rightarrow H$ is given by Eq.(1), with α replaced by the strong-coupling constant $\alpha_s(\mu_R^2)$ at the renormalization scale μ_R .

3.1 Square-root singularities

A square-root singularity is represented by a term containing a single inverse power of the threshold factor β_i ,

$$\beta_i = \sqrt{1 - 4 M_i^2 / M_H^2}, \quad \text{with} \quad M_i = M_W, M_Z, M_t. \quad (3)$$

In Ref. [5] it has been shown that square-root singularities are related to: i) derivatives of two-point one-loop functions, associated with Higgs WFR; ii) derivatives of three-point one-loop functions, generated by mass renormalization; iii) genuine irreducible two-loop diagrams containing a one-loop self-energy insertion. Therefore, in general, all three terms of Eq.(2) can show a β_i^{-1} behavior.

Concerning the Higgs WFR factor at one loop, we deal with the four mass patterns shown in Fig. 2; note that tadpole diagrams do not affect the threshold behavior. For the top-quark diagram, the coefficient of the derivative of the two-point one-loop function contains a positive power of the threshold factor β_t ; in other words, this diagram is β_t -protected at threshold. Consequently, \mathcal{A}^{WFR} of Eq.(2) contains, for both processes $H \rightarrow \gamma\gamma$ and $gg \rightarrow H$, square-root singularities only at the $2M_W$ and $2M_Z$ thresholds.

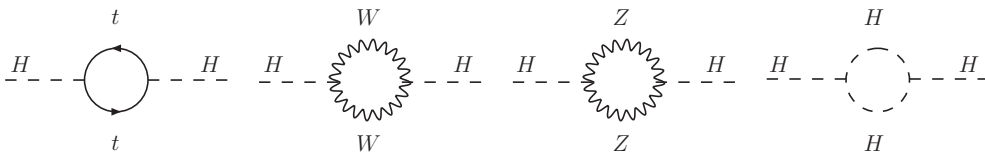


Figure 2: Sample diagrams for the Higgs wave-function renormalization factor at one loop.

We consider now genuine two-loop diagrams containing a self-energy insertion; they naturally join terms induced by one-loop mass renormalization as shown in Fig. 3, where bosonic and fermionic diagrams are illustrated. The bosonic component is obviously peculiar of the $H \rightarrow \gamma\gamma$ decay; in addition, we observe that only charged bosonic diagrams are present, because of the nature of the triple non-abelian gauge coupling in the Standard Model.

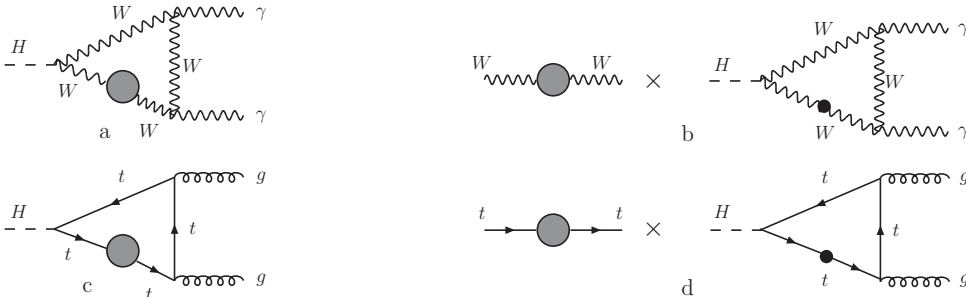


Figure 3: Two-loop and mass-renormalization diagrams relevant for the analysis of square-root singularities. Gray circles represent the sum of all one-loop two-point diagrams; black dots denote a derivative.

Fermionic diagrams are β_t -protected at threshold, and do not require any special care. The two-loop vertex containing a W self-energy insertion, and the associated W -mass renormalization contribution, lead instead to a β_W^{-1} -divergent behavior. However, the two-loop irreducible diagram of Fig. 3a can be cast in a representation where the singular part is completely written in terms of the one-loop diagrams of Fig. 3b. Moreover, it is possible to check explicitly that the unphysical β_W^{-1} behavior, generated by the two-loop diagram of Fig. 3a, exactly cancels the β_W^{-1} divergency

due to one-loop W -mass renormalization of Fig. 3b (performed in the complex-mass setup we are going to describe in Section 4).

This cancellation mechanism corroborates the general picture of Ref. [1]: self-energy insertions signal the presence of an unstable particle, and are the consequence of a misleading organization of the perturbative expansion; Dyson-resummed propagators should be used and complex poles should replace real masses as input data. The outcome of our analysis, performed at the algebraic level, is straightforward: at the amplitude level, only the inclusion of the Higgs WFR factor generates square-root singularities at the $2M_W$ and $2M_Z$ thresholds for both processes $H \rightarrow \gamma\gamma$ and $gg \rightarrow H$.

3.2 Logarithmic singularities

We briefly address here the issue of logarithmic singularities, given by terms containing a factor $\ln(-\beta_i^2 - i0)$, generated by the diagrams of Fig. 4. As thoroughly discussed in Ref. [5], the scalar configuration associated with the diagrams illustrated in Fig. 4 generates a logarithmic singularity. If the massive loop is made of top quarks, the scalar integral appears at the amplitude level with a multiplicative factor β_t^2 , and the logarithmic singularity is β_t^2 -protected at threshold. The same consideration is not valid for a W loop; here the logarithmic singularity can be viewed as the remnant of a Coulomb singularity in the one-loop sub-diagram.

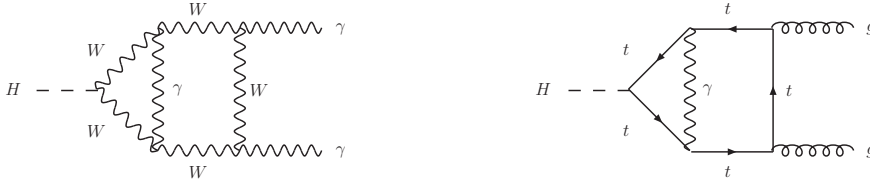


Figure 4: Irreducible two-loop vertex diagrams which can generate a logarithmic divergency.

4 Complex masses

A pragmatic gauge-invariant solution to the problem of threshold singularities due to unstable particles for the $H \rightarrow \gamma\gamma$ decay has been introduced and formalized in Ref. [5] (ad hoc introduction of a width is however common practice in the literature). After reviewing the corresponding scheme, termed in the following as minimal complex-mass (MCM) scheme, we will discuss the extension to the full complex-mass (CM) scheme, looking ahead to precise predictions for the production mechanism $gg \rightarrow H$.

4.1 Minimal complex-mass scheme

In the MCM scheme the NLO amplitude of Eq.(1) and Eq.(2) is decomposed according to

$$\mathcal{A}^{\text{NLO}} = \sum_{i=W,Z} \frac{A_{\text{SR},i}}{\beta_i} + A_{\text{LOG}} \ln(-\beta_W^2 - i0) + A_{\text{REM}}, \quad (4)$$

where square-root- ($A_{\text{SR},i}$) and logarithmic-singular (A_{LOG}) terms have been isolated from the component which is finite for $\beta_i \rightarrow 0$ (A_{REM}). From the discussion of Section 3, we know that $A_{\text{SR},i}$, with $i = W, Z$, is generated for both $H \rightarrow \gamma\gamma$ and $gg \rightarrow H$ by Higgs WFR at one loop; A_{LOG} shows up for $H \rightarrow \gamma\gamma$ only, and is induced by the bosonic diagram of Fig. 4.

After proving that all coefficients in Eq.(4), gauge-parameter independent by construction, satisfy the WST identities, we minimally modify the amplitude introducing the complex-mass scheme of Ref. [4] for the divergent terms. In principle, two steps are required: first, the real masses of the W and Z bosons, used as input data, are replaced by the corresponding complex poles in the threshold factors β_i , $i = W, Z$, and in the coefficients $A_{\text{SR},i}$ and A_{LOG} (also at the level of the couplings); second, the real parts of the W and Z self-energies stemming from mass renormalization at one loop are traded for the complete self-energies, including imaginary parts.

In practice, the second step amounts to a replacement of the conventional on-shell mass renormalization equation with the associated expression for the complex poles,

$$m_i^2 = M_i^2 \left[1 + \frac{G_F M_W^2}{2\sqrt{2}\pi^2} \text{Re}\Sigma_i^{(1)}(M_i^2) \right] \Rightarrow m_i^2 = s_i \left[1 + \frac{G_F s_W}{2\sqrt{2}\pi^2} \Sigma_i^{(1)}(s_i) \right], \quad (5)$$

where $\Sigma_i^{(1)}(M_i^2)$, with $i = W, Z$, denotes the W (Z) one-loop self-energy, and complex poles are defined as

$$s_i = \mu_i (\mu_i - i\gamma_i), \quad \mu_i^2 = M_i^2 - \Gamma_i^2, \quad \gamma_i = \Gamma_i \left(1 - \frac{\Gamma_i^2}{2M_i^2} \right). \quad (6)$$

Here M_i and Γ_i are the canonical on-shell values for the mass and the width of unstable gauge bosons.

Note that, concerning the W boson, the replacement of the real part of the self-energy with the full expression has to be performed also at the level of the Fermi-coupling renormalization equation, which becomes

$$g = 2 \left(\sqrt{2} G_F s_W \right)^{1/2} \left[1 - \frac{G_F s_W}{4\sqrt{2}\pi^2} \Delta \right], \quad \Delta = \Sigma_W^{(1)}(0) - \Sigma_W^{(1)}(s_W) + 6 + \frac{7 - 4s_\theta^2}{2s_\theta^2} \ln c_\theta^2. \quad (7)$$

Here g is the bare (or \overline{MS} -renormalized) weak-coupling constant, and the squared cosine of the weak-mixing angle $c_\theta^2 = \cos^2 \theta$ ($s_\theta^2 = \sin^2 \theta = 1 - c_\theta^2$) is fixed by $c_\theta^2 = \mu_W^2 / \mu_Z^2$.

Here it is important to note that the cancellation mechanism between two-loop diagrams and one-loop mass-renormalization terms generated by the decomposition of Fig. 3a,b, mentioned commenting Eq.(4), is a consequence of the introduction of Eq.(5) and does not take place in the conventional on-shell renormalization framework for real masses. This cancellation has a striking consequence: one-loop mass renormalization contributes only to the remainder A_{REM} , and the steps summarized in Eq.(5) and Eq.(7) are not required anymore.

The MCM scheme allows for a straightforward removal of unphysical infinities: real masses of unstable gauge bosons are traded for complex poles in divergent terms, gauge-parameter invariance and WST identities are preserved and the amplitude has a decent threshold behavior, as shown in Fig. 5 for the NLO electroweak corrections to the $H \rightarrow \gamma\gamma$ decay width. Here the dotted curve represents the result obtained using conventional on-shell masses for unstable gauge bosons as input data; the two-loop amplitude is artificially infinite at threshold and badly fails to approximate the correct result above threshold, as a consequence of the severe β_W^{-1} behavior of Eq.(4) (enhanced above threshold by the fact that the compensation illustrated in Fig. 3a,b does not occur in the pure real-mass setup).

A nice feature of the MCM scheme (dashed curve) is its simplicity: as a consequence of the cancellation mechanism taking place among divergent contributions, this scheme does not require any analytic continuation of two-point functions connected to mass renormalization to the unphysical Riemann sheet, because the replacement indicated in Eq.(5) is not needed. The MCM scheme,

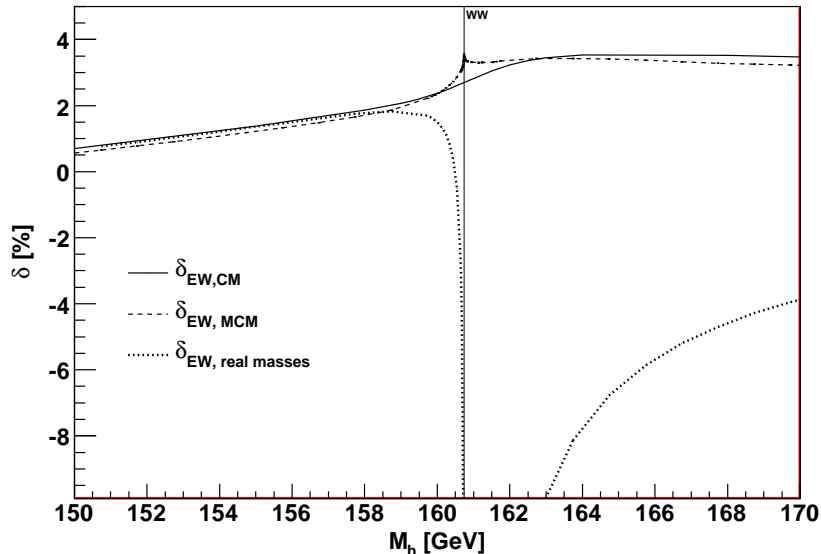


Figure 5: Percentage NLO electroweak corrections to the partial width for $H \rightarrow \gamma\gamma$; here $\Gamma^{\text{NLO}} = \Gamma^{\text{LO}}(1 + \delta_{\text{EW}})$. MCM (CM) scheme is described in Section 4.1 (4.2). Setup is described in Section 5.

however, does not deal with cusps associated with the crossing of normal thresholds, as shown in Fig. 5 for the WW threshold.

4.2 Complex-mass scheme

The large and artificial effects arising around normal thresholds in the MCM scheme or in a scheme where the masses of unstable particles are kept real (in this case the amplitude exactly diverges at threshold) are aesthetically unattractive. In addition, they represent a concrete problem in assessing the impact of two-loop electroweak corrections on processes relevant for the LHC. An important example is represented by Higgs production via gluon fusion: here, the large effect of NNLO QCD corrections naturally suggests to investigate possible sources of additional sizeable corrections.

We have therefore undertaken the task of introducing the complete complex-mass scheme of Ref. [4], as explained for a two-loop calculation in Ref. [8] (see also Ref. [12]), for evaluating two-loop electroweak corrections to the Standard Model processes $H \rightarrow \gamma\gamma$ and $gg \rightarrow H$. The procedure described in Section 4.1 for the divergent terms of Eq.(4) has been extended to the remainder A_{REM} . In particular, all two-loop diagrams have been computed with complex masses for the internal vector bosons relying on the techniques developed in Ref. [2,17].

In the full CM setup, the real parts of the W and Z self-energies induced by one-loop renormalization of the masses and the couplings have to be traded for the associated complex expressions by means of Eq.(5) and Eq.(7). However, we notice that:

i) for $H \rightarrow \gamma\gamma$, the Z boson self-energy connected to mass renormalization would arise only from the tree-level couplings of the photons, entailing an overall factor $g^2 s_\theta^2$ for the LO amplitude; in the CM scheme, in fact, s_θ^2 is expressed through the ratio of the vector-boson masses. However, because of our choice for the input-parameter set [5], the factor $g^2 s_\theta^2$ is re-absorbed by introducing the fine-structure constant α . In addition, as we said earlier, the electromagnetic coupling goes

unrenormalized, once WFR factors for on-shell photons are included.

ii) for $gg \rightarrow H$, Z mass renormalization clearly does not play any role. In addition, the tree-level coupling of the Higgs field to the top quark contains a factor g/M_W ; after combining the renormalization of the weak-coupling constant g , related to the Fermi-coupling constant through Eq.(7), with mass renormalization for the W boson, encoded in Eq.(5), the W self-energy evaluated at the complex pole drops out (see also Ref. [18]).

As a result, for $gg \rightarrow H$ it is enough to replace the real masses for the W and Z bosons with their complex poles, as usual also in the couplings; for $H \rightarrow \gamma\gamma$, one has also to trade the real part of the W self-energy for its full complex expression at the level of mass and coupling renormalization, via Eq.(5) and Eq.(7). The effect for the $H \rightarrow \gamma\gamma$ decay mode, shown in Fig. 5 (solid curve), is a full smoothing of the unphysical cusp associated with the WW threshold; although numerical negligible, it provides a benchmark for the $gg \rightarrow H$ study we will perform in Section 5.

The scheme can be easily extended to the fermionic sector replacing also the top-quark real mass by its complex pole. Since the behavior associated with the $t\bar{t}$ threshold is β_t -protected, we do not pursue this issue here.

The introduction of gauge-invariant complex poles for gauge bosons leads to technical complications, due to the fact that one- and two-loop integrals have to be computed with complex arguments. If only internal masses are complexified, the analytical continuation of loop integrals does not pose any additional problem; after writing the parametric representation of one- and two-loop diagrams, it is easy to control that squared masses have semi-positive definite coefficients; therefore the replacement $M^2 - i0 \rightarrow s_p = \mu^2 - i\mu\gamma$ is straightforward.

One-loop two-point functions arising in the reduction of the amplitude, instead, have to be carefully treated; here the external squared momentum can be complex and logarithms have to be extended to the second Riemann sheet. In general, the presence of complex momenta in two-loop diagrams demands an analytical continuation also for polylogarithms. In all cases, the correct analytical continuation is determined by the request that the value for a stable gauge boson should be smoothly approached when the coupling tends to zero. This is achieved starting from a complex argument, $z = z_R + i z_I$, defining $\tilde{z} = z_R - i0$, and replacing ordinary logarithms and polylogarithms with

$$\overline{\ln}(z; \tilde{z}) = \ln z - 2i\pi\theta(-z_R), \quad \overline{\text{Li}_2}(z; \tilde{z}) = \text{Li}_2(z) - 2i\pi \ln z_R \theta(z_R - 1). \quad (8)$$

4.3 External unstable particles

From a formal perspective, external unstable particles should not appear in any computation, since they cannot be included in the asymptotic states forming the bases of the Hilbert space. Concerning Higgs physics, however, available calculations deal with an external on-shell Higgs boson and do not perform the ultimate step of introducing a complex pole and the associated residue for the decaying Higgs [19].

For the production process $gg \rightarrow H$, we have verified that there are no practical problems associated with gauge-parameter invariance and WST identities once we deal with an on-shell Higgs. For the $H \rightarrow \gamma\gamma$ decay, there is a LO contribution containing the bare Higgs mass, represented by a charged Higgs-Kibble one-loop triangle diagram. Standard mass renormalization introduces the on-shell Higgs mass, through the real part of the one-loop two-point self-energy, and leads to a violation of the WST identities above the WW threshold. In both aforementioned MCM and CM schemes the real part of the Higgs self-energy stemming from mass renormalization is traded for the complex expression, even if the external Higgs boson is assumed to be an on-shell particle.

5 Numerical effects for Higgs production

The dominant production mechanism of the Standard Model Higgs boson at the LHC is the gluon fusion process, $gg \rightarrow H$: in this section we discuss the numerical impact at the two-particle vector-boson thresholds of the two-loop electroweak corrections in the framework of the MCM and CM schemes.

In the computation we have set light-fermion masses to zero and introduced the W and Z boson complex poles by means of Eq.(6). As input parameters we have used the following values taken from Ref. [20]:

$$\begin{aligned} M_W &= 80.398 \text{ GeV}, & M_Z &= 91.1876 \text{ GeV}, \\ \Gamma_Z &= 2.4952 \text{ GeV}, & G_F &= 1.16637 \times 10^{-5} \text{ GeV}^{-2}. \end{aligned} \quad (9)$$

For the mass of the top quark, we have used $M_t = 170.9 \text{ GeV}$ [21]; for the width of the W boson, we have chosen the value $\Gamma_W = 2.093 \text{ GeV}$, predicted by the Standard Model with electroweak and QCD corrections at one loop.

Our results for δ_{EW} , defined through $\sigma^{\text{EW}} = \sigma^{\text{LO}}(1 + \delta_{\text{EW}})$, are shown in Fig. 6, where we include the complete corrections, comprehensive of light- and top-quark contributions, comparing MCM and CM scheme. The corresponding numerical results are given in Tab. 1.

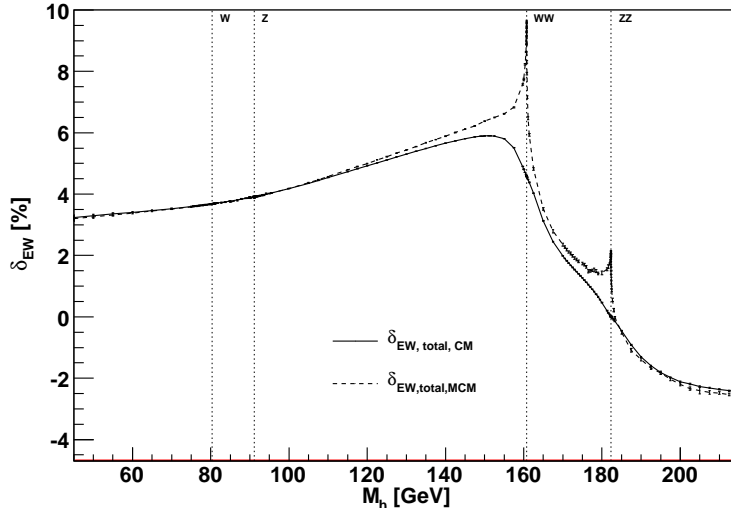


Figure 6: The two-loop electroweak percentage corrections for the total partonic cross section $\sigma(gg \rightarrow H)$. MCM (CM) scheme is described in Section 4.1 (4.2). Setup of Section 5.

In Fig. 7 we show the details of the region around the WW threshold, including the result obtained using purely real masses.

The numerical relevance of NLO electroweak corrections around the vector-boson thresholds depends crucially on the implementation of the renormalization scheme: the relative corrections in the MCM scheme reach about 10% (2%) at the WW (ZZ) threshold; in the CM scheme, they amount to 5% at the WW threshold and vanish at the ZZ one.

M_H	δ_{EW}^{MCM}	δ_{EW}^{CM}	M_H	δ_{EW}^{MCM}	δ_{EW}^{CM}	M_H	δ_{EW}^{MCM}	δ_{EW}^{CM}
140.0	5.88	5.66	162.5	4.82	4.03	180.0	1.43	0.47
145.0	6.12	5.80	165.0	3.52	3.13	182.5	0.96	- 0.02
150.0	6.38	5.90	167.5	2.79	2.45	185.0	- 0.50	- 0.46
152.5	6.50	5.89	170.0	2.35	1.99	187.5	- 1.09	- 0.91
155.0	6.62	5.81	172.5	1.99	1.61	190.0	- 1.39	- 1.31
157.5	6.83	5.51	175.0	1.74	1.27	195.0	- 1.82	- 1.82
160.0	7.72	4.82	177.5	1.51	0.90	200.0	- 2.20	- 2.11

Table 1: Percentage electroweak corrections in MCM (Section 4.1) and CM (Section 4.2) schemes as a function of the Higgs mass in GeV ($M_t = 170.9$ GeV).

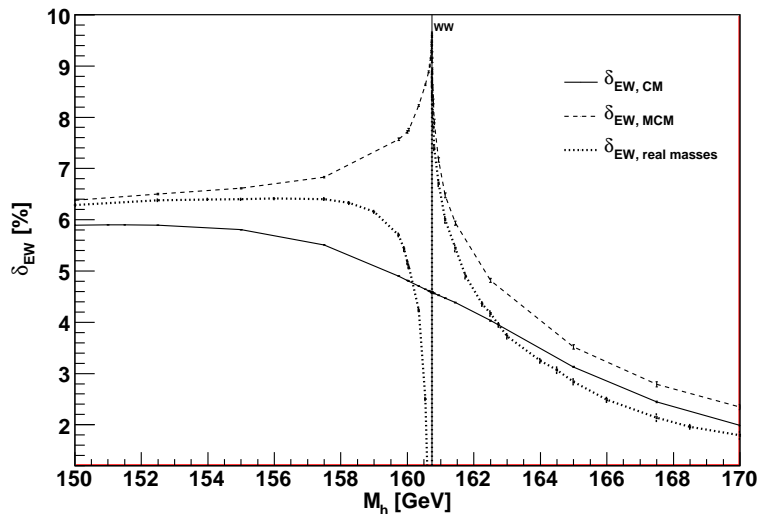


Figure 7: Same as Fig. 6, around the WW threshold. MCM (CM) scheme is described in Section 4.1 (4.2). Setup of Section 5.

6 Conclusions

In this paper we have considered the extension of the complex-mass scheme to two-loop multi-scale calculations. After discussing the general setup we have given numerical results for the two-loop percentage corrections to the $H \rightarrow \gamma\gamma$ and $gg \rightarrow H$ processes in the Standard Model around the vector-boson thresholds.

We have compared a minimal implementation of the complex-mass scheme and the complete one. For Higgs masses close to the WW and ZZ thresholds, NLO electroweak corrections can be considered under control only after a full implementation of the complex-mass scheme.

The electroweak scaling factor for the cross section does not exceed the +6% level in the range $100 \text{ GeV} < M_H < 200 \text{ GeV}$; incongruent +10% effects around thresholds are avoided, as a consequence of the complex-mass scheme employed.

Acknowledgments

Feynman diagrams have been drawn with the packages AXODRAW [22] and JAXODRAW [23]. The calculations performed in this paper have been performed with FORM [24].

References

- [1] M.J.G. Veltman, *Physica* **29** (1963) 186.
- [2] S. Actis, G. Passarino, C. Sturm and S. Uccirati, *NNLO Computational Techniques: the Cases $H \rightarrow \gamma\gamma, gg$* , in preparation.
- [3] M. Drees and K.i. Hikasa, *Phys. Rev. D* **41** (1990) 1547;
K. Melnikov, M. Spira and O.I. Yakovlev, *Z. Phys. C* **64** (1994) 401, hep-ph/9405301.
- [4] A. Denner, S. Dittmaier, M. Roth and L.H. Wieders, *Nucl. Phys. B* **724** (2005) 247, hep-ph/0505042;
A. Denner and S. Dittmaier, *Nucl. Phys. Proc. Suppl.* **160** (2006) 22, hep-ph/0605312;
A. Denner, S. Dittmaier, M. Roth and D. Wackerroth, *Nucl. Phys. B* **560** (1999) 33, hep-ph/9904472.
- [5] G. Passarino, C. Sturm and S. Uccirati, *Phys. Lett. B* **655** (2007) 298, arXiv:0707.1401 [hep-ph].
- [6] The CMS Collaboration, *Physics TDR Vol. II*, *J. Phys. G: Nucl. Part. Phys.* **34** (2007) 995.
- [7] N.E. Adam *et al.*, report of the *Working Group on Higgs Bosons* for the workshop *Physics at TeV Colliders*, Les Houches, France, 2007, arXiv:0803.1154 [hep-ph].
- [8] S. Actis and G. Passarino, *Nucl. Phys. B* **777** (2007) 100, hep-ph/0612124.
- [9] S. Actis, G. Passarino, C. Sturm and S. Uccirati, *NLO Electroweak Corrections to Higgs Boson Production at Hadron Colliders*, PITHA 08/20, SFB/CP-08-62, TTP08-38.
- [10] J.C. Ward, *Phys. Rev.* **78** (1950) 182;
A.A. Slavnov, *Theor. Math. Phys.* **10** (1972) 99 [*Teor. Mat. Fiz.* **10** (1972) 153];
J.C. Taylor, *Nucl. Phys. B* **33** (1971) 436.
- [11] W. Beenakker *et al.*, *Nucl. Phys. B* **500** (1997) 255, hep-ph/9612260;
E.N. Argyres *et al.*, *Phys. Lett. B* **358** (1995) 339, hep-ph/9507216.
- [12] S. Actis, A. Ferroglia, M. Passera and G. Passarino, *Nucl. Phys. B* **777** (2007) 1, hep-ph/0612122;
S. Actis and G. Passarino, *Nucl. Phys. B* **777** (2007) 35, hep-ph/0612123.
- [13] M. Beneke, P. Falgari, C. Schwinn, A. Signer and G. Zanderighi, *Nucl. Phys. B* **792** (2008) 89, arXiv:0707.0773 [hep-ph];
S. Actis, M. Beneke, P. Falgari and C. Schwinn, arXiv:0807.0102 [hep-ph].
- [14] L.D. Landau, *Nucl. Phys.* **13** (1959) 181.

- [15] S. Gorla and G. Passarino, contribution to the proceedings of the DESY workshop *Loops and Legs in Quantum Field Theory 2008*, Sondershausen, Germany, 2008, arXiv:0807.0698 [hep-ph].
- [16] F. Boudjema and L.D. Ninh, arXiv:0806.1498 [hep-ph].
- [17] G. Passarino, Nucl. Phys. B **619** (2001) 257, hep-ph/0108252;
 G. Passarino and S. Uccirati, Nucl. Phys. B **629** (2002) 97, hep-ph/0112004; Nucl. Phys. B **747** (2006) 113, hep-ph/0603121;
 A. Ferroglia, M. Passera, G. Passarino and S. Uccirati, Nucl. Phys. B **680** (2004) 199, hep-ph/0311186;
 S. Actis, A. Ferroglia, G. Passarino, M. Passera and S. Uccirati, Nucl. Phys. B **703** (2004) 3, hep-ph/0402132.
- [18] G. Degrossi and F. Maltoni, Phys. Lett. B **600** (2004) 255, hep-ph/0407249.
- [19] B.A. Kniehl and A. Sirlin, Phys. Lett. B **530** (2002) 129, hep-ph/0110296;
 P.A. Grassi, B.A. Kniehl and A. Sirlin, Phys. Rev. D **65** (2002) 085001, hep-ph/0109228;
 B.A. Kniehl, C.P. Palisoc and A. Sirlin, Phys. Rev. D **66** (2002) 057902, hep-ph/0205304.
- [20] C. Amsler *et al.* [Particle Data Group], Phys. Lett. B **667** (2008) 1.
- [21] The CDF and D0 Collaborations, FERMILAB-TM-2380-E, hep-ex/0703034.
- [22] J.A.M. Vermaseren, Comput. Phys. Commun. **83** (1994) 45.
- [23] D. Binosi and L. Theussl, Comput. Phys. Commun. **161** (2004) 76, hep-ph/0309015.
- [24] J.A.M. Vermaseren, math-ph/0010025.